Gravity and the Direction of Time

An AI-Assisted Audit of Reversibility, Janus Structures, Curvature, Black-Hole Area Growth, and a Collision-Induced Complexity Tail

Keiji Yoshimura
Independent researcher
keiji.yoshimura.research@gmail.com

Technical monograph / reproducibility audit
Version 1.0.1 – 23 August 2026

Status and claim boundary. This is an AI-assisted, non-peer-reviewed technical monograph. It does not propose a new theory of time or gravity, does not claim that gravity selects a fundamental future direction, and makes no claim of worldwide priority for the mathematical corollary derived in Sections 7.2–7.3. Its purpose is to place a versioned exploratory audit, negative results, reproducibility checks, and a narrowly stated mathematical consequence into a single inspectable record.

Prepared for open e-print dissemination.

Abstract

This monograph consolidates a five-stage AI-assisted audit that began with a deliberately broad question: whether the direction of time, the local "time axis," and gravity could be related in a way stronger than the standard relations already encoded in general relativity, Hamiltonian mechanics, statistical mechanics, and quantum theory. The audit progressively tested and narrowed that intuition rather than constructing a new model. Local Lorentz symmetry and the time-reversal covariance of the ADM constraints provide no universal metric-only rule that selects one timelike cone as future. Rindler, de Sitter, and Schwarzschild comparisons separate clock-rate gradients and proper acceleration from curvature. Closed finite-level quantum clocks can lose path visibility through proper-time correlations yet are exactly refocused by an ideal echo, whereas residual loss appears only after an open reduced channel is introduced. Newtonian many-body calculations distinguish a rigorous scale minimum for suitable nonnegative-energy Janus sectors from non-monotonic, measure- and horizon-dependent shape-complexity statistics. A natural mass-metric measure for the equal-mass planar three-body shape sphere was reconstructed and mapped back to Newtonian trajectories; it yields two statistically symmetric structural branches rather than a dynamically preferred future. Public GW250114 release products were also used to reproduce the collaboration-defined black-hole area-growth statistic, while showing why a future-horizon area law is not a fundamental time-orientation selector.

A mathematical by-product is isolated and proved: under the BKM mass-metric shape probability, normalized three-body shape complexity has a collision-induced tail

$$P(Q > q) = \frac{1}{6q^2} + \frac{2\sqrt{6}}{27q^3} + O\left(q^{-4}\right),$$

so moments are finite exactly below order two and the truncated second moment grows as $(1/3) log T + O(1)$. The ingredients of this result are published; targeted searches did not locate this exact probability-and-moment statement, so it is presented only as a potentially unreported elementary corollary, not a priority claim. Overall, the audit supports a strong relation between gravity and proper time, curvature, causal structure, and structural arrows, but finds no evidence that standard gravity itself creates or selects a unique fundamental future direction.

Keywords: arrow of time; general relativity; proper time; Janus point; shape dynamics; three-body problem; gravitational complexity; quantum clocks; black-hole area theorem; reproducibility; AI-assisted research.

1 Purpose, origin, and claim hierarchy

The project began from a broad conceptual intuition rather than a proposed theory: perhaps the notions of a temporal direction, a local time axis, and gravity were connected more deeply than the familiar statement that gravity affects clocks. The research protocol was therefore exploratory and adversarial. A proposed connection was retained only when it survived counterexamples, time-reversal tests, numerical checks, or comparison with public data. Null results and boundary failures were preserved rather than repaired by adding free parameters.

Throughout the audit, six notions that are often compressed into the word "time" were kept distinct:

1. coordinate time t;
2. proper time τ measured along a worldline;
3. time orientation, i.e. a continuous selection of one of the two timelike cone halves;
4. thermodynamic arrows produced by coarse graining, records, and low-entropy boundary conditions;
5. structural arrows such as clustering or shape-complexity growth away from a Janus point;
6. future-horizon area growth in black-hole mechanics.

The final claim hierarchy is intentionally asymmetric. The audit strongly supports the standard relation between gravity and proper time, causal structure, tides, and black-hole mechanics. It conditionally supports two-sided structural arrows in restricted Newtonian models. It does *not* support a law by which the metric or gravitational field alone chooses one fundamental future direction.

Known microscopic T violation in the weak interaction is not denied here; direct T violation has been observed in the neutral-B system [7]. The present question is narrower: whether the gravitational metric itself supplies a universal rule that distinguishes one timelike-cone half as the fundamental future.

2 Versioned audit design and reproducibility strategy

Five computational stages were produced. Each release retained source code, machine-readable tables, validation outputs, manifests, and SHA-256 inventories. Later stages did not silently overwrite earlier negative or ambiguous results.

Audit-stage summary

v0.1: Connected the intuition to proper-time gradients, Raychaudhuri kinematics, FLRW time reversal, and a regularized Newtonian Janus-point toy model. Demonstrated practical irreversibility from chaos without fundamental microscopic time asymmetry.

v0.2: Replaced hand-imposed Janus initial conditions by event finding in exact dynamics; separated global complexity from local morphology; verified Liouville/symplectic volume preservation; distinguished finite-level clock dephasing from irreversible dynamics.

v0.3: Added a local metric-only time-orientation no-go argument, ADM time reversal checks, an acceleration/curvature separation, mass-ratio, and energy-sector Janus tests, negative-energy Kepler counterexamples, multilevel clocks, and a public-data audit of GW250114 black-hole area growth.

v0.4: Tested ideal clock/path echo versus an open Markov channel, constructed a symmetric three-clock curvature discriminator, and audited Janus statistics against observation horizon and section weighting.

v0.5: Reconstructed the BKM mass-metric measure, tested coordinate invariance and metric dependence, analysed the collision tail, and sampled actual Newtonian three-body trajectories from that measure.

The externally stored release hashes were:

- v0.1: 80570999087ac89737c587067fde0fb44ea925ab0ed564873da164c3e906ed9f
- v0.2: a5f9f9da699bcbb06211a93d4ead580f3523e19b937a33eac0328129d4b92cb6
- v0.3: 4793bdf68af0ab9b365c3f0132665905386386d7e69bcf32ff932bfae49496fb
- v0.4: 39b11a2f07fce4e4d86f84dc76ea19f5c01d4b3324a344f1a3b9d043978986ca
- v0.5: 14340724a95899aba90d53688033897d22063fcbaecc9995c88bc1e39e47b32e

The novelty-audit archive and the candidate-B final-audit archive have SHA-256 values 87e6ccbb5679946d84bee83a427bee716ec317466c29abf3a47bef9a848d570b and 1f46d9490306fe72b1336c036c9072659b03739d6f755969ebfaf3c9078a01f8, respectively.

3 Relativity: clocks, local acceleration, curvature, and time orientation

3.1 Proper time is physical; coordinate time is not a selector

For a static line element written as

$$ds^2 = -N^2c^2dt^2 + h_{ij}dx^i dx^j,$$

a stationary clock satisfies $d\tau = Ndt$, while the proper acceleration of a static observer obeys

$$a_i = c^2 D_i \ln N.$$

This is a real and measurable relation between gravity, acceleration, and clock rates. It is not, however, a rule that identifies one time orientation as the future.

In the weak terrestrial field the audit reproduced the gravitational clock gradient at approximately 1.09×10^{-19} per millimetre, consistent with millimetre-scale optical-clock measurements at the 10^{-19} scale [6]. This establishes that the originating intuition had contact with real clock physics, but not that a “tilted time axis” is identical to spacetime curvature.

3.2 Why the metric does not choose the future cone

At any event a Lorentzian metric can be placed in local Minkowski form,

$$g_{ab} = diag(-1, 1, 1, 1).$$

Replacing a timelike basis vector e_0 by $-e_0$ leaves the metric unchanged while exchanging the two timelike cone halves. Curvature tensors can identify preferred timelike eigendirections in special spacetimes, but eigenvectors retain the sign ambiguity $u^a \leftrightarrow -u^a$. Thus no universal local functional of the metric alone can label one cone half as "future" in all Lorentzian spacetimes. Time-orientability is a global property: in a time-orientable spacetime the metric determines the causal-cone structure, but it does not by itself distinguish one of the two globally consistent time orientations as "future". Choosing one orientation requires additional structure or convention, for example a matter flow, a clock field, or asymmetric boundary data.

The same conclusion appears in the ADM formulation of the gravitational constraints [4]. In a standard sign convention,

$$^{(3)}R + K^2 - K_{ij}K^{ij} = 16\pi G\rho,$$

$$D_j\left(K^{ij} - \gamma^{ij}K\right) = 8\pi G j^i.$$

Under

$$\gamma_{ij} \to \gamma_{ij}, \quad K_{ij} \to -K_{ij}, \quad \rho \to \rho, \quad j^i \to -j^i,$$

the Hamiltonian constraint is unchanged and the momentum constraint changes sign on both sides. A 4096-case algebraic implementation check gave a maximum residual of 8.88×10^{-16}. This numerical check does not discover the symmetry; it verifies that the implemented transformation respects the known equations.

3.3 Clock-rate gradient versus curvature

Rindler spacetime [2] supplies a direct counterexample to identifying a lapse gradient with curvature: accelerated stationary clocks have a spatial clock-rate gradient in flat spacetime. Conversely, spatially flat FLRW slicing of de Sitter spacetime can have unit lapse and zero comoving proper acceleration while curvature is nonzero. The two concepts are therefore inequivalent in both directions.

The v0.3-v0.4 analysis sharpened this separation by locally matching proper acceleration in a flat Rindler frame and in Schwarzschild spacetime. The local quadratic structure is the standard tidal structure exposed by Fermi-normal expansions [5]. Using geometrized units $G = c = 1$, around a reference radius r_0, with outward proper distance s and normalization $N(0) = 1$,

$$N(s) = 1 + as - \frac{M}{r_0^3}s^2 + O\left(s^3\right).$$

The matched Rindler lapse contains the constant and linear terms but not the quadratic tidal term. A symmetric three-clock combination

$$\delta_2 N = \frac{N(+L)+N(-L)}{2} - N(0)$$

therefore cancels the constant and acceleration pieces, leaving

$$\delta_2 N_{Schw} \simeq -\frac{M}{r_0^3}L^2, \qquad \delta_2 N_{Rindler} = 0.$$

This is a curvature discriminator, not a time-direction discriminator.

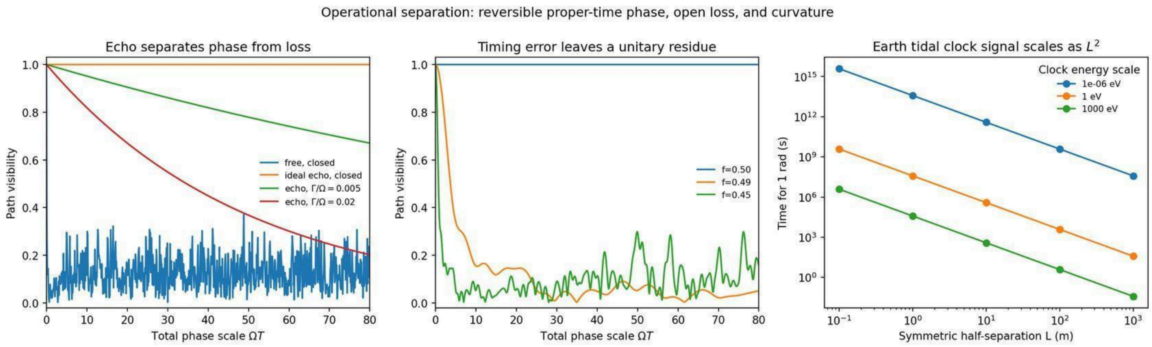

v0.4 audit of clock/path echo and acceleration-cancelled curvature discrimination. The figure is generated from the archived audit code and is presented as a diagnostic summary rather than experimental data.

4 Quantum clocks: proper-time correlation is not fundamental irreversibility

For a path degree of freedom coupled to an internal finite-level clock with energies E_n and probabilities p_n, the path visibility after a proper-time difference $\Delta\tau$ can be written in the proper-time interferometric form discussed in [10, 11]:

$$V(\Delta\tau) = \left|\sum_n p_n e^{-iE_n \Delta\tau/\hbar}\right|.$$

It is exactly even:

$$V(-\ \Delta\tau) = V(\Delta\tau).$$

The v0.3 audit compared two-level, harmonic 16-level, anharmonic 16-level, and irregular 64-level spectra. Long apparent dephasing can occur without visible natural recurrence over a finite observation window, yet the complete finite system remains pure and can be exactly reversed by the inverse unitary.

v0.4 turned this observation into an operational echo test, applying the refocusing logic of spin echo [8] to the path–internal-clock model. If the paths are exchanged at a fraction f of the total protocol, the residual proper-time difference becomes

$$\Delta\tau_{eff} = (2f\ -\ 1)\Delta\tau.$$

At the ideal midpoint, $f\ =\ 1/2$, all deterministic internal phases refocus simultaneously. A full $128\ \times\ 128$ density-matrix calculation for the 64-level clock found a maximum ideal-echo visibility error $2.22\ \times 10^{-16}$ and a maximum difference between the matrix calculation and analytic expression $1.25\ \times 10^{-14}$.

By contrast, after adding a reduced Markov pure-dephasing channel of the standard quantum-dynamical-semigroup type [9],

$$\rho_{01}(T) \mapsto e^{-\Gamma T}\rho_{01}(T),$$

the echo removes the deterministic clock phase but not environmental decoherence. For the test point $\Gamma/\Omega\ =\ 0.02$ and $\Omega T\ =\ 40$, the residual factor was 0.44933. The forward channel was completely positive, whereas the formal inverse had a negative Choi eigenvalue $(-\ 0.61277)$ and therefore was not a physical CPTP inverse on arbitrary states. This establishes an arrow in the *reduced open-system model*; it does not establish fundamental nonunitarity of the full system, nor does it make the residual specifically gravitational. This interpretation boundary is consistent with published criticism of overly universal gravitational-decoherence claims [12].

5 Newtonian Janus structures: theorem, counterexamples, and statistics

5.1 The conditional scale-minimum theorem

Let

$$I = \sum_i m_i \left| r_i - r_{cm} \right|^2, \qquad D = \tfrac{1}{2}\dot{I}.$$

For a Newtonian potential $V < 0$ homogeneous of degree -1, the Lagrange–Jacobi identity gives the scale-convexity structure used in Janus-point analyses [13, 15]:

$$\ddot{I} = 4E - 2V, \qquad \dot{D} = 2E - V.$$

For collision-free evolution with $E \geq 0$, $\dot{D} > 0$. Therefore $D = 0$ can occur at most once; if it occurs, it is a strict minimum of the scale I. This is a rigorous statement about scale convexity. It is not a theorem that shape complexity is monotonic, and it does not select which temporal branch should be called future.

5.2 Negative energy is a real boundary, not a numerical nuisance

v0.3 explicitly tested positive, zero, and negative energy sectors. The unconditional statement “Newtonian gravity always creates one Janus point” is false. In a negative-energy Kepler ellipse, $D = 0$ recurs; in a circular orbit $D = 0$ and I is constant for all times. These are exact counterexamples, not finite-sample exceptions.

For nonnegative-energy many-body samples, the scale theorem remained robust while shape complexity behaved statistically. In the $E = 0$ equal-mass ensembles, terminal complexity ratios strengthened from $N = 3$ to $N = 8, 16, 32$, but no branch among the larger pooled set was pointwise monotonic at every sampled time. Mass ratios up to $100:1$ and increasing positive energy altered the fraction and magnitude of later complexity growth without invalidating the scale minimum. This is evidence that the scale statement and the structural-arrow statistic are different claims.

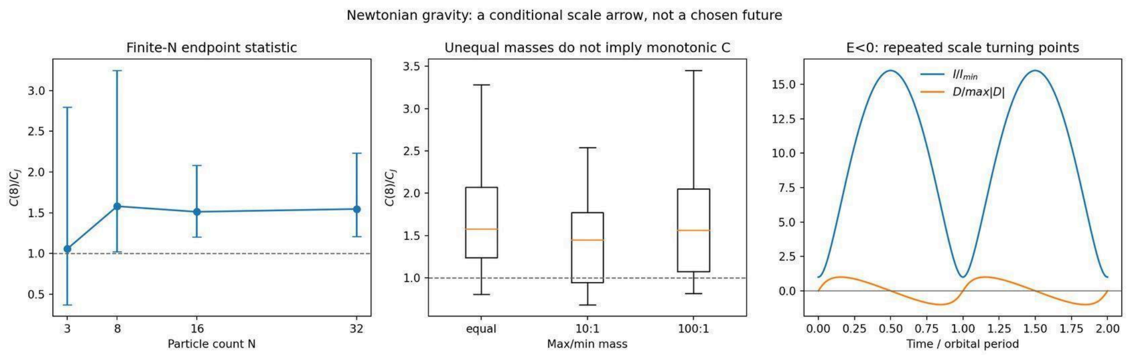

v0.3 boundary audit for Newtonian Janus structures. The numerical results support the conditional scale theorem while showing finite-N, mass, energy, and non-monotonic shape-complexity effects.

5.3 Observation horizon and section weighting

Building on the BKM typicality/Janus framework [14], v0.4 fixed $E = P = L = D = 0, I = 1$ for equal-mass $N = 8$ exact $1/r$ dynamics and compared three weights on the Janus section: equal event count, a near-section residence weight $1/\dot{D}_J = 1/C_J$, and a flux-like weight $\dot{D}_J = C_J$. At a central close-pair cutoff, the weighted fraction with $C(T) > C_J$ increased from about 82% at $T = 2$ to about 96% at $T = 8$. The horizon difference was clear in a clustered bootstrap, while the tested close-pair cutoff effect remained unresolved and the section-weight difference was detectable but small. Consequently, a numerical “probability of complexity growth” is conditional on a counting rule and observation horizon; it is not a universal constant supplied by the equations alone.

6 Natural measure, collision boundary, and sampled three-body dynamics

6.1 Finite mass-metric probability and its non-uniqueness

For the equal-mass planar three-body problem, quotienting translations, rotations, and scale gives the familiar shape-sphere description [19, 22]. With the mass metric,

$$ds^2 = d\psi^2 + sin^2\psi\, d\phi^2,$$

and a unit cotangent direction represented by χ, the projectivized mass-metric probability can be normalized as

$$dP = \frac{sin\psi}{4\pi^2}\, d\psi\, d\phi\, d\chi, \quad 0 \leq \chi < \pi.$$

The shape marginal is uniform sphere area. Two independent sphere samplers yielded a two-sample KS statistic 0.002328, whereas an intentionally wrong sampler omitting the $sin\psi$ Jacobian gave 0.20854.

The measure is finite, but “natural” does not mean unique from topology or projective structure alone. BKM explicitly note non-uniqueness before choosing the dynamically motivated mass metric [14]; related shape-space work likewise treats a metric choice as physical input. The v0.5 stress test used the smooth permutation-invariant conformal family

$$g_\alpha = e^{\alpha m} g_{mass}, \qquad m = 6 \sum_{a<b} \left(f_{ab} - \frac{1}{3}\right)^2, \qquad f_{ab} = \frac{r_{ab}^2}{\sum_{c<d} r_{cd}^2}.$$

This is the exact morphology coordinate used in the archived v0.5 code: it is zero at equilateral shapes and approaches one at a binary-collision shape. The conformal reweighting produced substantial changes in typical complexity quantiles even though each resulting measure remained finite and coordinate invariant. This does not refute the mass metric; it shows that typicality predictions include a physical metric choice.

6.2 Collision measure and divergent high moments

With $I_{cm} = 1$, define normalized shape complexity

$$Q = \frac{1}{3} \sum_{a<b} \frac{1}{r_{ab}}.$$

Near a binary-collision point at spherical angular distance δ, the Newtonian shape potential has the familiar collision singularity [22, 20], so $Q \propto \delta^{-1}$ while the local area element scales as $\delta\, d\delta$. Thus collision points have zero probability measure, yet singular observables can have divergent high moments.

A 2-million-shape Monte Carlo audit found a fitted survival-tail slope -2.09246 against the geometric expectation -2, a close-pair probability slope $+2.01134$ against $+2$, and a winsorized second-moment fit linear in $logT$ with $R^2 = 0.99882$. The numerical results serve as checks of the analytic asymptotics developed in Section 7.2. In particular, the archived tail table approaches the analytic prediction $q^2 P(Q > q) \rightarrow 1/6$ at large q; the theorem does not rely on the fitted log–log slope.

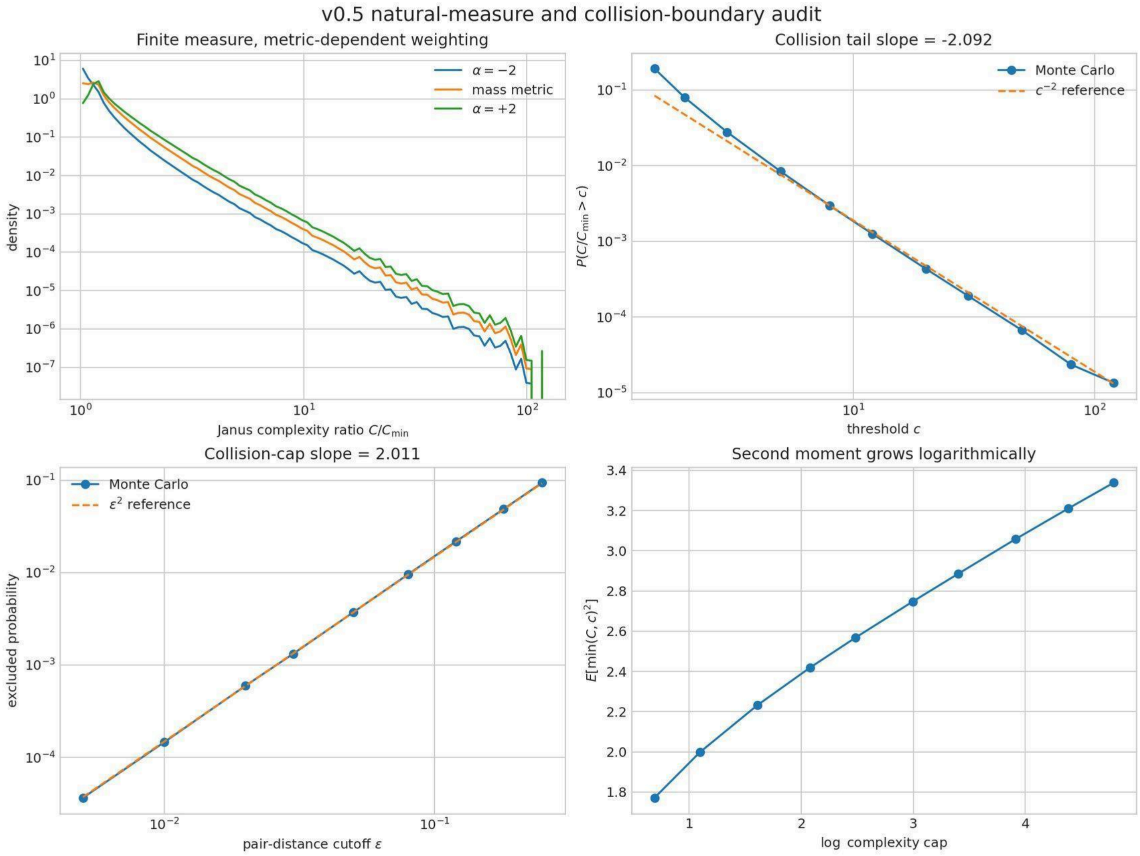

v0.5 shape-measure and collision-boundary audit. The finite mass-metric probability coexists with a collision-induced heavy tail in the unbounded complexity observable.

6.3 Mapping the natural measure back to Newtonian trajectories

v0.5 also sampled actual Newtonian initial data from the mass-metric shape measure. Using mass-weighted Jacobi coordinates, each shape was represented at $I_{cm} = 1$, a horizontal cotangent direction was sampled, and the velocity magnitude was set so that $E = P = L = D = 0$. From 128 solutions, both velocity signs were integrated, giving 256 branches.

By $t = 240$, 249 branches (97.27%) satisfied the predeclared classification as a bound binary plus an outward escaper. No collision guard was reached. The maximum reported relative energy drift was 3.19×10^{-7}. The exact velocity-reversal construction provides the primary branch-exchange symmetry: changing v to $-v$ interchanges the two branches of the same solution. Finite-sample comparisons of classification time, binary eccentricity, and the tested alignment statistic found no detectable implementation-induced or finite-horizon preference, but these non-significant tests are diagnostics rather than proofs of distributional identity. Velocity reversal exchanges the two structural “futures” rather than identifying one as fundamental.

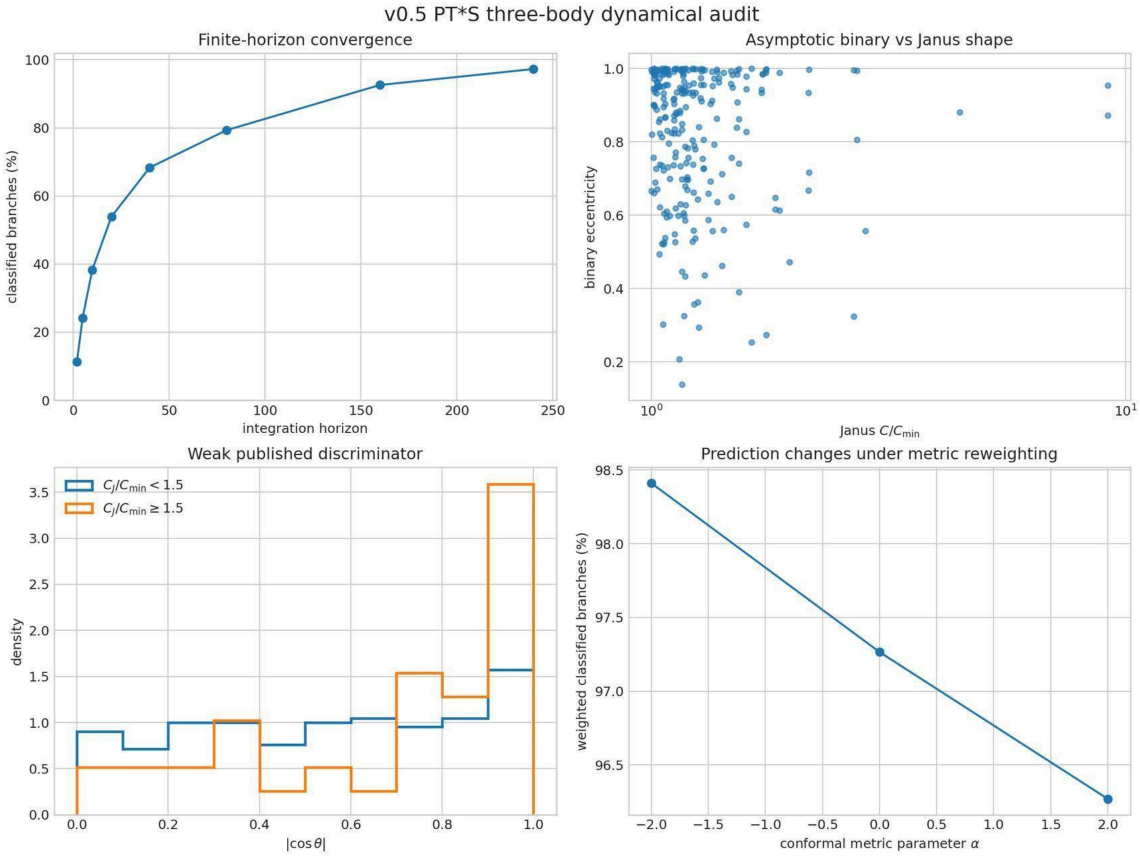

v0.5 three-body dynamics sampled from the reconstructed mass-metric shape probability. Most branches reach a hierarchical binary-plus-escaper state within the finite integration horizon, with no preferred velocity-sign branch.

7 A collision-induced heavy tail on the planar three-body shape sphere

This section records the narrow mathematical by-product that survived the novelty audit. The proof uses published ingredients – the round shape-sphere geometry [19], the BKM mass-metric probability [14], and Newtonian collision singularities in shape variables [22, 20] – but the explicit probability and moment statement below was not located in the targeted primary-literature search. No claim of priority is made.

7.1 Conventions

Take three labeled equal point masses in the plane with $G = m_1 = m_2 = m_3 = 1$, center of mass zero, and $I_{cm} = 1$. Define mass-weighted Jacobi vectors

$$\rho_1 = \frac{r_2 - r_1}{\sqrt{2}}, \qquad \rho_2 = \sqrt{\frac{2}{3}}\left(r_3 - \frac{r_1 + r_2}{2}\right).$$

The Hopf vector $n \in S^2$ is

$$n_1 = |\rho_1|^2 - |\rho_2|^2, \quad n_2 = 2\rho_1 \cdot \rho_2, \quad n_3 = 2\rho_1 \times \rho_2.$$

Let

$$B_{12} = (-1, 0, 0), \quad B_{31} = \left(\frac{1}{2}, -\frac{\sqrt{3}}{2}, 0\right), \quad B_{23} = \left(\frac{1}{2}, \frac{\sqrt{3}}{2}, 0\right).$$

Then the mutual distances obey

$$r_{ab}(n)^2 = 1 - n \cdot B_{ab},$$

and the B_{ab} are the binary-collision shapes. Define

$$Q(n) = \frac{1}{3}\left(\frac{1}{r_{12}(n)} + \frac{1}{r_{23}(n)} + \frac{1}{r_{31}(n)}\right).$$

For these conventions, $Q = C_S/C_{S,min}$ and $Q \geq 1$, with equality at the equilateral shapes.

The BKM mass-metric measure on PT^*S has uniform shape marginal

$$d\mu(n) = \frac{dA(n)}{4\pi}.$$

7.2 Main theorem

Theorem. As $q \to \infty$,

$$P(Q > q) = \frac{1}{6q^2} + \frac{2\sqrt{6}}{27q^3} + O\left(q^{-4}\right).$$

Consequently, for $p \geq 0$,

$$E\left[Q^p\right] < \infty \quad \Leftrightarrow \quad p < 2.$$

Moreover, for $Q_T = min(Q, T)$, there is a finite constant κ such that

$$E\left[Q_T^2\right] = \frac{1}{3} log T + \kappa + O\left(T^{-1}\right).$$

Thus Q has finite mean but infinite second moment and variance.

Proof. Fix B_{12} and let δ be the central angle from it. Then

$$r_{12} = \sqrt{1 - cos\delta} = \sqrt{2} sin(\delta/2).$$

At the collision point the other two distances both equal $\sqrt{3/2}$. Their contributions are smooth and non-singular, so in geodesic polar coordinates one may write, uniformly in the polar angle θ,

$$Q(\delta, \theta) = \frac{a}{\delta} + b + \delta c(\delta, \theta), \qquad a = \frac{\sqrt{2}}{3}, \quad b = \frac{2\sqrt{6}}{9},$$

where c is bounded and smooth for sufficiently small δ. Hence $\partial_\delta Q = - a/\delta^2 + O(1)$ uniformly in θ, so for sufficiently large q the superlevel component around the collision point has a unique polar boundary. Uniform inversion gives

$$\delta_q(\theta) = \frac{a}{q} + \frac{ab}{q^2} + O\left(q^{-3}\right).$$

Outside disjoint neighborhoods of the three collision points, Q is bounded, so the high-q superlevel set is exactly the union of three congruent collision components. Their normalized area is

$$P(Q > q) = 3\frac{1}{4\pi}\int_0^{2\pi}\left(1 - cos\delta_q(\theta)\right)d\theta = 3\left(\frac{a^2}{4q^2} + \frac{a^2 b}{2q^3} + O\left(q^{-4}\right)\right) = \frac{1}{6q^2} + \frac{2\sqrt{6}}{27q^3} + O\left(q^{-4}\right).$$

For $p > 0$, the layer-cake identity

$$E\left[Q^p\right] = p\int_0^\infty q^{p-1} P(Q > q)\, dq$$

converges at infinity exactly for $p < 2$; $p = 0$ is trivial. Finally,

$$E\left[min(Q, T)^2\right] = 2\int_0^T q\, P(Q > q)\, dq,$$

and the tail expansion gives

$$2qP(Q > q) - \frac{1}{3q} = O\left(q^{-2}\right),$$

which is integrable. Hence the logarithmic expression follows. ▫

7.3 General surface lemma and quotient corollary

The tail exponent is not a coordinate accident. Let (M, g) be a compact smooth Riemannian surface with finitely many points B_i, and let a probability μ have continuous area density w. If a nonnegative F is bounded away from the B_i and

$$F(x) = \frac{a_i}{d_g(x, B_i)} + O(1), \qquad a_i > 0,$$

near each singular point, then

$$\mu(F > q) \sim \frac{\pi}{q^2} \sum_i w(B_i) a_i^2.$$

If all $w(B_i) > 0$, the moment threshold is again $p = 2$. Hence the exponent and moment boundary survive any smooth positive reweighting at collision, although the leading coefficient changes.

For finite symmetry operations acting on the shape sphere, such as orientation reversal or equal-mass label permutations, let $\pi: S^2 \to S^2/\Gamma$ be the quotient map. If both μ and Q are invariant under Γ, then with $\mu^- = \pi_* \mu$ and $Q = Q^- \circ \pi$,

$$\mu^-(Q^- > q) = \mu(Q > q)$$

exactly. No separate hemisphere or orbifold-boundary cap count is required for these shape-space quotients.

Projective momentum identification acts instead on the cotangent-fiber degree of freedom, not on the shape sphere itself. Because Q depends only on shape and the BKM shape marginal is obtained after integrating over the projective momentum direction, that fiber identification does not alter the distribution of Q.

8 Black-hole area growth: a conditional arrow, not a fundamental selector

Black-hole mechanics provides one of the strongest real gravitational phenomena with a directional statement; the classical area theorem is due to Hawking [29], and an earlier observational test used GW150914 [30]. The v0.3 audit used the GW250114 area-law paper [31] together with the official public code/data release and its published checksums [32]. The collaboration-defined area statistic was reproduced, including the baseline reported value of approximately 4.4σ. Independently recomputing Kerr areas from the released posterior arrays gave, for the baseline analysis,

$$X = \frac{\mu_f - \mu_i}{\sqrt{\sigma_f^2 + \sigma_i^2}} = 4.447211,$$

which rounds to 4.4σ. Sensitivity scans also reproduced the published approximately 3.4σ and 3.6σ variants.

A direct empirical-tail count from the same finite posterior arrays gave a different one-sided normal equivalent (about 3.755σ). This was not treated as a correction to the published result because the collaboration explicitly defines the quoted statistic from the first two moments rather than from a sparse posterior tail, and the pairwise combinations are not independent experimental repetitions.

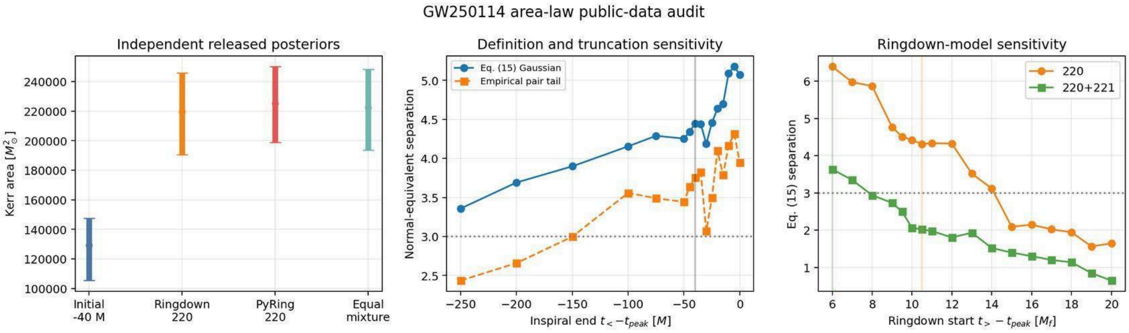

v0.3 audit of the GW250114 public black-hole area products. The baseline collaboration-defined statistic is reproduced from released arrays; the exercise is not a new strain-level Bayesian parameter-estimation analysis.

The conceptual boundary remains essential. Hawking's classical area theorem [29] is stated for a *future* event horizon under energy and global regularity assumptions. Time reversal maps a black-hole merger to a white-hole-type history with the opposite horizon orientation; the Einstein equations do not locally reject the reversed solution merely because its temporal label is opposite. GW250114 therefore supplies strong conditional evidence for area growth in the observed black-hole boundary conditions, not evidence that the gravitational field equation itself selects the universe's fundamental future cone.

9 What survived, what failed, and why the audit stopped

Final claim audit

Claim: Gravity affects clock rates and proper time
Status: Supported / established
Reason: Standard general relativity and precision-clock observations.

Claim: A lapse gradient or "time-axis tilt" is curvature itself
Status: Rejected
Reason: Flat Rindler and curved de Sitter/Schwarzschild counterexamples.

Claim: The metric alone universally chooses the future cone
Status: Rejected as a universal local rule
Reason: Local Lorentz sign ambiguity; ADM time-reversal covariance.

Claim: Closed proper-time clock dephasing is fundamentally irreversible
Status: Rejected in the tested finite models
Reason: Exact inverse unitary and ideal echo restore coherence.

Claim: Open-system residual loss can define an effective arrow
Status: Conditionally supported
Reason: Reduced Markov channels need not have a physical CPTP inverse; not uniquely gravitational.

Claim: Newtonian gravity always produces one Janus point
Status: Rejected unconditionally
Reason: Negative-energy Kepler ellipse and circular-orbit counterexamples.

Claim: For collision-free Newtonian motion, an existing is a unique scale minimum
Status: Supported / conditional theorem
Reason: Lagrange–Jacobi identity.

Claim: Shape complexity increases monotonically on every branch
Status: Rejected
Reason: Finite- numerical branches fluctuate; statistics depend on horizon and measure.

Claim: The BKM three-body mass-metric measure is finite
Status: Supported in the specified model
Reason: Explicit normalization on .

Claim: That measure is uniquely forced by projective structure alone
Status: Rejected
Reason: Published non-uniqueness; alternate smooth metrics alter typicality numbers.

Claim: Black-hole area growth is supported by GW250114 public products
Status: Strong conditional support
Reason: Published and independently reconstructed release-level statistic.

Claim: Black-hole area growth proves gravity selects fundamental future
Status: Unsupported
Reason: Future-horizon orientation and boundary conditions enter the theorem.

Claim: A new law of gravitational time orientation is required
Status: No
Reason: All audited effects are accounted for by established frameworks.

The audit stopped because further seed counts, clock levels, or repetitions of the same toy systems would not create new discriminatory power. Meaningful continuation would require external input: a real interferometer error budget, a deployable curvature-clock geometry, a well-defined relativistic or quantum model with new observables, a physically selected large-N measure, or a concrete new hypothesis predicting a sign-sensitive deviation from standard theory.

10 Novelty boundary and publication position

A dedicated literature audit compared three possible publication claims. The metric-dependence of the BKM natural measure is already acknowledged in the source literature, so it is not a new conceptual result. The asymptotic alignment relation in the three-body model was already numerically studied by BKM with a larger ensemble; the present calculation is an independent reproduction rather than a discovery.

The collision-tail theorem in Section 7 survived only as a narrow candidate. The targeted search located the published ingredients – the shape sphere, binary-collision geometry, the BKM measure, and the divergence of complexity – but did not locate a primary source stating the same $1/\left(6q^2\right)$ coefficient, the all-orders moment threshold, and the logarithmic truncated-second-moment asymptotic as one theorem. Because the proof is short once the published geometry is assembled, absence from the targeted search is *not* evidence of priority. The appropriate label is therefore: **potentially unreported elementary corollary; novelty unverified**.

Accordingly this monograph does not present the result as a standalone new theory or as a major independent paper. It records the theorem together with the entire audit path that produced and then narrowed it.

11 AI assistance, human oversight, and responsibility

This project used substantial assistance from OpenAI Codex/ChatGPT. Across the archived stages, AI assistance included literature retrieval, algebraic derivation, code generation, numerical execution, interpretation, figure generation from computed data, validation logic, novelty searches, and manuscript drafting.

The human author supplied the originating research question, directed continuation and stopping decisions, requested adversarial audits and claim-boundary checks, selected which outputs should be retained or rejected, and decided the publication posture. The author does not present himself as a professional specialist in general relativity, celestial mechanics, or shape dynamics, and does not claim to have independently re-derived every equation without AI assistance.

The safeguards built into the project include deterministic seeds where applicable, explicit solver tolerances, preservation of negative/null results, machine-readable outputs, independent output validators within each release, SHA-256 inventories, and a separate novelty/final-audit stage. These safeguards are not a substitute for independent expert review. Readers are explicitly invited to check the derivations, code, and source attribution.

12 Data and code availability

The underlying project consists of versioned reproducibility packages v0.1-v0.5 plus novelty and final-audit packages. Each package contains some combination of source code, CSV/JSON outputs, figures, validation records, manifests, environment notes, and SHA-256 inventories. Large third-party GW250114 data are not redistributed; the audit records the official public source and checksum information needed to reacquire them.

Because ai.viXra accepts a single PDF rather than supplemental files, this monograph contains the scientific claims and the final theorem in self-contained form. The reproducibility archives are retained by the author and identified by the SHA-256 values listed in Section 2. A persistent public repository or DOI should be cited here once the packages are deposited; no repository URL is asserted in this version.

13 Conclusion

The initial intuition – that gravity, temporal direction, and a “time axis” might reflect one deeper mechanism – did not survive in that strong form. The audit instead separated several distinct facts. Gravity controls proper-time relations, causal cones, tidal curvature, structure formation, and black-hole mechanics. Time-symmetric equations can support two-sided structural arrows around a Janus point, while open-system approximations can support effective irreversible arrows. Neither result supplies a universal rule selecting one fundamental future direction from the metric alone.

The most concrete new-looking mathematical residue is much narrower: in the equal-mass planar Newtonian three-body shape sphere under the BKM mass-metric probability, the point-particle collision singularities induce a q^{-2} complexity tail, finite moments only below order two, and logarithmic divergence of the truncated second moment. This is recorded as an explicit technical corollary of known ingredients, with novelty deliberately left unclaimed.

The scientific value of the project is therefore primarily diagnostic and reproducibility-oriented: a broad speculative question was progressively narrowed by counterexamples, exact identities, controlled numerical experiments, public-data reproduction, and a final literature audit until only bounded claims remained.

References

[1] A. Raychaudhuri, “Relativistic cosmology. I,” Phys. Rev. 98, 1123 (1955). https://doi.org/10.1103/PhysRev.98.1123
[2] W. Rindler, “Hyperbolic motion in curved space time,” Phys. Rev. 119, 2082 (1960). https://doi.org/10.1103/PhysRev.119.2082
[3] R. V. Pound and G. A. Rebka Jr., “Apparent weight of photons,” Phys. Rev. Lett. 4, 337 (1960). https://doi.org/10.1103/PhysRevLett.4.337
[4] R. Arnowitt, S. Deser, and C. W. Misner, “The dynamics of general relativity,” in Gravitation: An Introduction to Current Research, edited by L. Witten (Wiley, New York, 1962), pp. 227–264; republication: arXiv:gr-qc/0405109. https://arxiv.org/abs/gr-qc/0405109
[5] F. K. Manasse and C. W. Misner, “Fermi normal coordinates and some basic concepts in differential geometry,” J. Math. Phys. 4, 735 (1963). https://doi.org/10.1063/1.1724316
[6] T. Bothwell et al., “Resolving the gravitational redshift across a millimetre-scale atomic sample,” Nature 602, 420–424 (2022). https://doi.org/10.1038/s41586-021-04349-7
[7] BABAR Collaboration, “Observation of time-reversal violation in the B^0 meson system,” Phys. Rev. Lett. 109, 211801 (2012). https://doi.org/10.1103/PhysRevLett.109.211801
[8] E. L. Hahn, “Spin echoes,” Phys. Rev. 80, 580 (1950). https://doi.org/10.1103/PhysRev.80.580
[9] G. Lindblad, “On the generators of quantum dynamical semigroups,” Commun. Math. Phys. 48, 119–130 (1976). https://doi.org/10.1007/BF01608499
[10] M. Zych et al., “Quantum interferometric visibility as a witness of general relativistic proper time,” Nat. Commun. 2, 505 (2011). https://doi.org/10.1038/ncomms1498
[11] I. Pikovski et al., “Universal decoherence due to gravitational time dilation,” Nat. Phys. 11, 668–672 (2015). https://doi.org/10.1038/nphys3366
[12] Y. Bonder, E. Okon, and D. Sudarsky, “Can gravity account for the emergence of classicality?” Phys. Rev. D 92, 124050 (2015). https://doi.org/10.1103/PhysRevD.92.124050
[13] J. Barbour, T. Koslowski, and F. Mercati, “Identification of a gravitational arrow of time,” Phys. Rev. Lett. 113, 181101 (2014). https://doi.org/10.1103/PhysRevLett.113.181101
[14] J. Barbour, T. Koslowski, and F. Mercati, “Entropy and the typicality of universes,” arXiv:1507.06498v2 (2015). https://arxiv.org/abs/1507.06498
[15] J. Barbour, T. Koslowski, and F. Mercati, “Janus points and arrows of time,” arXiv:1604.03956 (2016). https://arxiv.org/abs/1604.03956
[16] H. D. Zeh, “Comment on the `Janus Point' explanation of the arrow of time,” arXiv:1601.02790 (2016). https://arxiv.org/abs/1601.02790
[17] D. Lazarovici and P. Reichert, “Arrow(s) of time without a past hypothesis,” arXiv:1809.04646v3 (2018). https://arxiv.org/abs/1809.04646
[18] J. S. Schiffrin and R. M. Wald, “Measure and probability in cosmology,” Phys. Rev. D 86, 023521 (2012). https://doi.org/10.1103/PhysRevD.86.023521
[19] R. Moeckel and R. Montgomery, “Symmetric regularization, reduction and blow-up of the planar three-body problem,” Pac. J. Math. 262, 129–189 (2013). https://doi.org/10.2140/pjm.2013.262.129
[20] G. S. Krishnaswami and H. Senapati, “Curvature and geodesic instabilities in a geometrical approach to the planar three-body problem,” J. Math. Phys. 57, 102901 (2016). https://doi.org/10.1063/1.4964340
[21] L. Sydnes, Geometric reduction and the three body problem, doctoral thesis, NTNU (2012). https://hdl.handle.net/11250/258996
[22] F. Mercati and P. Reichert, “Total collisions in the N-body shape space,” Symmetry 13, 1712 (2021). https://doi.org/10.3390/sym13091712
[23] S. Fleischer and A. Knauf, “Improbability of collisions in n-body systems,” arXiv:1802.08564 (2018). https://arxiv.org/abs/1802.08564
[24] J. Barbour, Z. Doborjginidze, T. Koslowski, and H. Shukla, “Complexity and its creation,” arXiv:2405.07480 (2024). https://arxiv.org/abs/2405.07480
[25] Y. Dandekar and B. Kol, “Distribution of regularized three-body phase-volume,” Celest. Mech. Dyn. Astron. 137, 32 (2025). https://doi.org/10.1007/s10569-025-10262-2
[26] M. I. R. Lourenço, J. Barbour, and F. S. N. Lobo, “Scale invariance, variety and central configurations,” arXiv:2602.11225 (2026). https://arxiv.org/abs/2602.11225
[27] J. Barbour, F. S. N. Lobo, and M. I. R. Lourenço, “Structural morphology and the gravitational arrow of time,” arXiv:2607.27526 (2026). https://arxiv.org/abs/2607.27526
[28] J. D. Bekenstein, “Black holes and entropy,” Phys. Rev. D 7, 2333 (1973). https://doi.org/10.1103/PhysRevD.7.2333
[29] S. W. Hawking, “Gravitational radiation from colliding black holes,” Phys. Rev. Lett. 26, 1344 (1971). https://doi.org/10.1103/PhysRevLett.26.1344
[30] M. Isi, W. M. Farr, M. Giesler, M. A. Scheel, and S. A. Teukolsky, “Testing the black-hole area law with GW150914,” Phys. Rev. Lett. 127, 011103 (2021). https://doi.org/10.1103/PhysRevLett.127.011103
[31] A. G. Abac et al. (LIGO Scientific, Virgo, and KAGRA Collaborations), “GW250114: Testing Hawking's Area Law and the Kerr Nature of Black Holes,” Phys. Rev. Lett. 135, 111403 (2025). DOI: 10.1103/kw5g-d732; arXiv:2509.08054. https://doi.org/10.1103/kw5g-d732
[32] LIGO Scientific Collaboration, Virgo Collaboration, and KAGRA Collaboration, “GW250114 discovery paper figure scripts,” Zenodo (2025). DOI: 10.5281/zenodo.16877102. https://doi.org/10.5281/zenodo.16877102